

SHAFTS: A Hybrid Approach for 3D Molecular Similarity Calculation. 2. Prospective Case Study in the Discovery of Diverse p90 Ribosomal S6 Protein Kinase 2 Inhibitors To Suppress Cell Migration

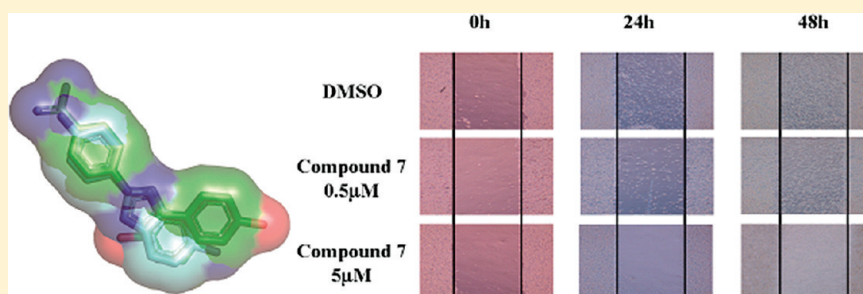
Weiqliang Lu,^{†,§} Xiaofeng Liu,^{†,§} Xianwen Cao,[†] Mengzhu Xue,[†] Kangdong Liu,^{*,†} Zhenjiang Zhao,[†] Xu Shen,[†] Hualiang Jiang,[†] Yufang Xu,[†] Jin Huang,^{*,†} and Honglin Li^{*,†}

[†]State Key Laboratory of Bioreactor Engineering, Shanghai Key Laboratory of Chemical Biology, School of Pharmacy, East China University of Science and Technology, Shanghai 200237, China

[‡]The Basic Medical College, Zhengzhou University, Zhengzhou 450001, China

S Supporting Information

ABSTRACT:



We described a prospective application of ligand-based virtual screening program SHAFTS to discover novel inhibitors for p90 ribosomal S6 protein kinase 2 (RSK2). Taking the putative 3D conformations of two weakly binding RSK2 NTKD inhibitors as query templates, SHAFTS was used to perform 3D similarity based virtual screening because of a lack of crystal structure of RSK2 protein, thus leading to the identification of several novel scaffolds that would have been missed by conventional 2D fingerprint methods. The most potent hit compounds show low micromolar inhibitory activities against RSK2. In particular, one of the hit compounds exhibits potent antimigration activity against the MDA-MB-231 tumor cell. The results exemplified SHAFTS' application in active enrichment and scaffold hopping, which is of general interest for lead identification in drug discovery endeavors and also provides novel scaffolds that lay the foundation for uncovering new RSK2 regulatory mechanisms.

INTRODUCTION

RSK2 is a member of the p90 ribosomal S6 kinase (RSK) family that regulates diverse cellular processes, such as cell growth, motility, survival, proliferation, and transformation.¹ RSKs are growth-factor-regulated serine/threonine kinases that lie downstream of Ras/mitogen-activated protein kinase (MAPK) pathway. The activation of RSKs is a multiple and sequential phosphorylation process involved in extracellular signal-regulated kinase-1/2 (ERK1/2) and 3-phosphoinositide-dependent protein kinase-1 (PDK-1).² This family contains four human isoforms (RSK1–4), and each is a product of a separate gene. Each RSK isoform consists of two distinct functional kinase domains, the N-terminal kinase domain (NTKD) and the C-terminal kinase domain (CTKD), which are connected by a linker region.³ CTKD is involved in autophosphorylation of RSK2, while NTKD is responsible for phosphorylating exogenous substrates at serine/threonine residues.⁴ The RSK2 phosphorylation substrates include transcription factors like cyclic AMP response element-binding protein (CREB), estrogen receptor- α (ER α), nuclear

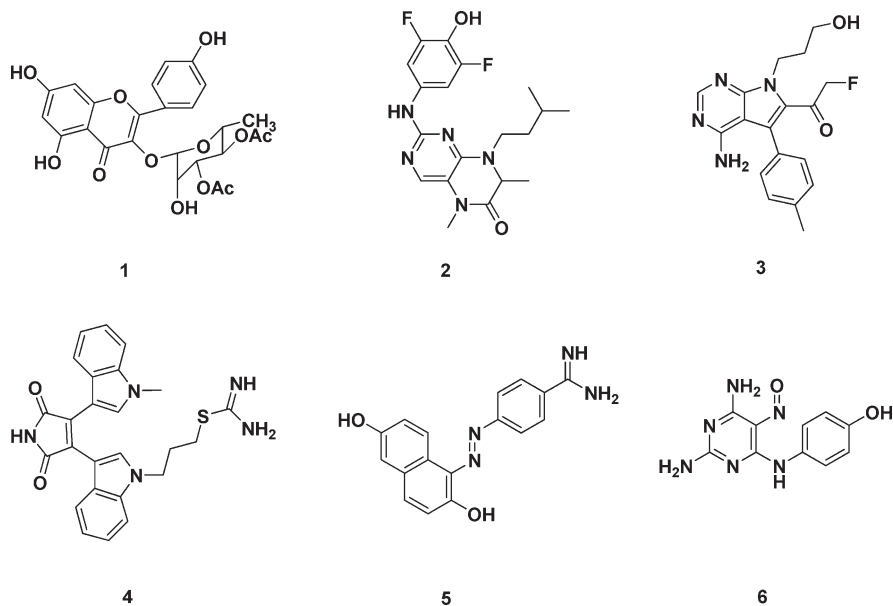
factor of activated T-cells 3 (NFAT3), and activating transcription factor 4 (ATF4).^{5–8}

Mutations in RSK2 have been shown to be responsible for Coffin–Lowry syndrome (CLS), which is an X-linked mental retardation condition associated with skeletal abnormalities.⁵ Overexpression and aberrant activation of RSK2 have been linked to many human diseases, including breast cancer, prostate cancer, and human head and neck squamous cell carcinoma. Furthermore, there are emerging and compelling evidence indicated a link between RSK2 and cell migration. RSK2 was identified as a principal effector of the RAS-ERK pathway in the regulation of mesenchymal motility and invasive capacities in non-transformed epithelial and carcinoma cells.⁹ A genome-wide RNAi screen was performed to uncover multiple RSK2-dependent regulation mechanisms of breast cell migration.¹⁰ In addition, RSK2 promotes the human head and neck squamous cell carcinoma cells

Received: January 26, 2011

Published: April 13, 2011

Chart 1. Selected Structures of Reported RSK2 Inhibitors



invasion and metastasis both in vitro and in vivo.¹¹ These studies suggest that RSK2 is a promising target for cancer metastasis and treatment and highlights the fact that developing specific and potent RSK2 inhibitors is of both research and clinical interest.¹²

To date, a number of potent RSK2 inhibitors have been reported (as shown in Chart 1).¹³ SL0101 **1** is the first reported RSK2 specific inhibitor that was extracted from the tropical plant *Forsteronia refracta* and exhibits excellent inhibitory activity ($IC_{50} = 89$ nM).^{14–16} This kaempferol glycoside exerts antiproliferative activity against the human breast cancer cell line, MCF-7, but has no effect on the normal breast cell line, MCF-10A.¹⁶ BI-D1870 **2** is a remarkably specific potent inhibitor for the RSK family (RSK1, RSK2, RSK3, and RSK4) with an in vitro IC_{50} of 10–30 nM, but it does not significantly inhibit 10 other AGC family kinases (cAMP-dependent protein kinases A, cGMP-dependent protein kinases G, and phospholipid-dependent protein kinases C).¹⁷ It decreased RSK-mediated phosphorylations of its downstream substrates, glycogen synthase kinase-3 β (GSK3 β), and LKB1 in cells. FMK **3** is a highly specific RSK inhibitor with an in vitro IC_{50} of 15 nM. Unlike **1** and **2**, it is an irreversible inhibitor of RSK through binding to the CTKD by deriving its potent kinase activity from the covalent addition of its chloromethylketone functionality to the thiol group of Cys436 located in the ATP pocket of the RSK2 CTKD and preventing the self-activation of NTKD.¹⁸ Ro31-8220 **4** is a classical PKC inhibitor and was shown to be a potent but nonspecific RSK2 inhibitor with IC_{50} of 36 nM.¹³ These four inhibitors were widely applied for elucidating the biochemistry of the RSK2 signaling pathway as chemical probes, but none of them have been applicable in clinical use. Hence, there are continually growing needs to discover novel RSK2 inhibitors for further development into therapeutic candidates for cancer treatment.

Although RSK2 has been proved to be a promising cancer therapeutic target, its 3D crystal structure has not yet been determined, rendering structure-based virtual screening of inhibitors very difficult to perform even though an atomic homology model has been reported.¹⁹ On the other hand, as mentioned above, the identified RSK2 inhibitors are not enough for building

a reliable pharmacophore model for pharmacophore matching based virtual screening. Taking advantage of their homology model, Nguyen et al. identified two novel weakly binding RSK2 inhibitors NSC356821 **5** and NSC51023 **6** via hierarchical virtual screening consisting of pharmacophore modeling and molecular docking.¹⁹ However, the volume of the ATP binding pocket in their model was manually expanded to tolerate larger nonspecific inhibitors like **4**. So rather than relying on the assumed information contained in the existing molecules and the nature of the corresponding interaction with the RSK2 NTKD region, a new 3D similarity based computational virtual screening procedure that maximizes both shape and chemical feature superposition between molecules was used to identify novel inhibitor scaffolds, which could fill in the similar binding volume of the ATP-binding site and result in comparable binding affinity with the RSK2 NTKD region.

Recently we developed SHAFTS, a hybrid 3D similarity calculation method, with its performance in retrospective virtual screening to enrich known actives and corresponding chemotypes from decoys for multiple target sets (unpublished results). This paper describes the first prospective application of SHAFTS in a successful discovery of novel inhibitors for the NTKD region of RSK2 kinase. Starting from two weakly binding inhibitors as the query templates, 16 compounds with IC_{50} lower than 20 μ M were identified as RSK2 inhibitors via chemotype switching directed by SHAFTS calculation, which are not expected to be discovered by conventional 2D similarity calculation. The three most potent hit compounds show low micromolar inhibitory activities against RSK2 and exhibited selectivity across a panel of related kinases. In particular, compound **7** possesses strong ex vivo and in vitro RSK2 binding ability and also exhibits potent antimigration activity against MDA-MB-231 tumor cells.

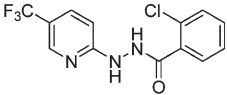
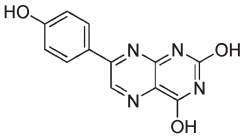
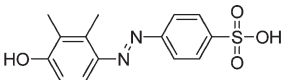
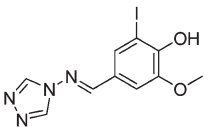
EXPERIMENTAL METHODS

3D Hybrid Similarity Calculation. SHAFTS was used to perform 3D similarity based virtual screening in this study. SHAFTS adopts a hybrid similarity metric of molecular shape and colored (labeled)

Table 1. Structures, SHAFTS Similarities, and Potencies of RSK2 Inhibitors

Compd.	Structure	Template ^a	SHAFTS ^b	ROCS ^b	ECFP_4 ^c	MACCS ^c	IC ₅₀ (μ M) ^d
7		5	1.108	0.896	0.061	0.428	0.32
8		6	1.401	1.085	0.222	0.482	0.48
9		6	1.071	0.747	0.147	0.328	0.95
10		5	1.089	0.896	0.077	0.318	1.06
11		5	1.053	1.025	0.136	0.511	1.38
12		6	1.276	1.214	0.298	0.6	1.58
13		5	1.157	0.846	0.061	0.34	2.88
14		6	1.26	1.063	0.143	0.491	3.03
15		5	1.256	1.029	0.288	0.561	3.47
16		5	1.185	0.981	0.207	0.365	5.50
17		5	1.157	0.803	0.167	0.521	7.04
18		6	1.136	0.996	0.167	0.566	9.99

Table 1. Continued

Compd.	Structure	Template ^a	SHAFTS ^b	ROCS ^b	ECFP_4 ^c	MACCS ^c	IC ₅₀ (μ M) ^d
19		6	1.062	0.823	0.108	0.433	13.18
20		5	1.084	0.914	0.133	0.388	14.45
21		5	1.219	0.935	0.232	0.421	15.14
22		5	1.023	0.811	0.121	0.461	16.18
4	-	-	-	-	-	-	0.010

^aThe hit compounds were selected with either 5 or 6 as the template in SHAFTS-based virtual screening. ^bThe SHAFTS and ROCS (combo score) similarities are in the range 0.0–2.0. ^cThe ECFP_4 and MACCS 2D similarity indexes are in the range 0.0–1.0. ^dIC₅₀ values were measured if the inhibition rate at 10 μ M was larger than 30%. IC₅₀ values are determined from the results of at least three independent tests of RSK2 kinase activity.

chemistry groups annotated by pharmacophore features for 3D similarity calculation and ranking, which is designed to integrate the strength of both pharmacophore matching and volumetric similarity approaches. A brief description of the SHAFTS method is given below, and the details of the algorithm and implementation can be found in Supporting Information and accessed at <http://59.78.96.61:8080/chemmapper/download.html>.

The hybrid similarity used to score and rank alignment modes and target molecules consists of the shape-densities overlap (ShapeScore) and chemical feature fit values (FeatureScore). For ShapeScore, the overlap of shape between molecules A and B can be defined as the sum of the overlap integrals of individual atomic shape-densities expressed in a Gaussian function and is normalized to [0, 1] using the cosine similarity metric. FeatureScore is essentially the fit value between the pharmacophore models extracted from template and target molecules, which is defined as the sum of the overlap between the feature points in molecules A and B with the same type and also normalized to [0, 1] using the cosine similarity metric. The hybrid similarity is the weighted sum of FeatureScore and ShapeScore with the default weighting factor of 1.0 and scaled to [0, 2].

$$\text{HybridScore} = \text{ShapeScore} + (w)(\text{FeatureScore}) \quad (1)$$

SHAFTS implements the feature triplet hashing method from PharmMapper server²⁰ for fast molecular overlay poses enumeration, and the optimal superposition between the target and the query molecules can be prioritized by calculating corresponding hybrid similarities. The higher HybridScore implies the better alignment pose in terms of both shape and chemotype identities between the query and target molecules.

Query Templates. Rather than starting from potent and specific inhibitors like 2 and 3, we preferred small chemical structures and fragment-like molecules (MW < 300) as the query templates because of their potential for rapid expansion and their potential for optimization into leads and then into preclinical candidates. As a result, two weakly binding RSK2 inhibitors 5 and 6 were selected as the queries, which are more rigid and smaller than other inhibitors and for which scaffold hopping is easy to perform with our method. Unfortunately there are no experimentally determined 3D conformations for these two templates; however, it is not compulsory for SHAFTS to start with the experimental bioactive conformers. Therefore the predicted binding poses of the two queries described along with a RSK2 homology model¹⁹ were adopted as the “quasi bioactive conformers” (as shown in Figure S1).

Database Preparation. The SPECS screening collection²¹ and MayBridge screening collection²² were used as the compound source for virtual screening. All the compounds containing inorganic atoms were removed prior to the screening. The remaining molecules are prepared (including adding hydrogen atoms, ionizing at the pH range from 5.1 to 9.1, and generating stereoisomers and valid single 3D conformers) by means of the LigPrep.²³ Since SHAFTS uses a semirigid strategy to characterize molecular flexibility, the conformational ensembles of corresponding target molecules in the database have to be generated prior to similarity calculation. Cyndi, a multiobjective evolution algorithm based conformation analysis program described previously,²⁴ was used to generate conformational ensembles (a maximum size of 200 conformers within 10 kcal/mol of the lowest conformer was kept) for each molecule in the databases.

Scaffold Hopping and Virtual Screening. Taking the structures of 5 and 6 as the queries, SHAFTS was used to search the

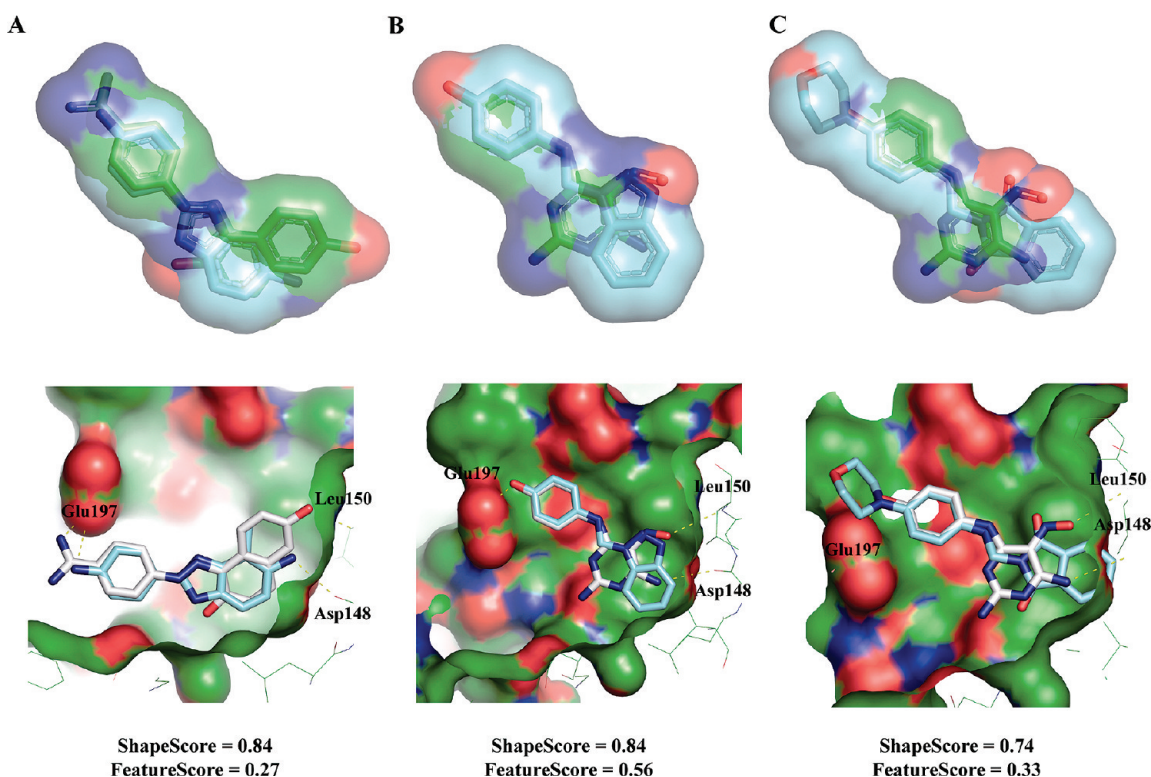


Figure 1. Superposition poses of the most potent hit compounds onto the templates and putative interaction modes with the homology model of RSK2 NTKD generated by SHAFTS: (A) 7 onto 5, (B) 8 onto 6, and (C) 9 onto 6. The corresponding ShapeScore and FeatureScore, which consist of SHAFTS similarity, are also annotated. The molecules and molecular surfaces are colored according to atom types (green and white for template carbons, cyan for hit carbons, red for oxygen, and blue for nitrogen), and the predicted intermolecular hydrogen bonds are depicted as yellow dash lines.

conformation databases, and only the best ranked conformer was reserved per molecule. The top 500 molecules with similarity of >1.0 were reserved for each template and each vendor database respectively, which resulted in 370 hits for template 5 and 389 hits for template 6 in SPECS and 500 hits for template 5 and template 6 in MayBridge, respectively. After visual analysis of the alignment poses between the hits and the templates (including the overall shape overlay and the chemotype overlays between the key functional groups on the templates and the corresponding ones from the hits), 156 candidates out of the 1759 compounds were purchased and tested in the RSK2 NTKD inhibitory assay.

Chemistry. All compounds were commercially available and purchased from SPECS and MayBridge, and the purities of compounds were determined by HPLC using an Agilent 1200 series instrument equipped with a Diamonsil-C18 column (250 mm × 4.6 mm, 5 μm particle size) and a UV/vis detector setting of λ = 254 nm. All compounds were eluted with the two solvent systems [CH₃OH as organic phase in method I and CH₃CN (or CH₃CN plus CH₃OH) as organic phase in method II] listed in Table S1 at a flow rate of 1 mL/min unless otherwise specified. HPLC analysis of the compounds assayed confirmed the purity at ≥95%.

In Vitro Kinase Inhibition Assay. The ADP Quest (DiscoverRx) was performed in 96-well flat-bottom plates in a 40 μL reaction volume according to the manufacturer's instructions. The kinase (20 ng, Millipore) in 30 μL assay buffer (15 mM HEPES, pH 7.4, 20 mM NaCl, 1 mM EGTA, 0.02% Tween 20, 10 mM MgCl₂, and 0.1 mg/mL BGG) containing 25 μM S6 peptide (AKRRRLSSLRA, Anaspec) was incubated for 20 min at room temperature with the indicated concentrations of the compounds to be tested. Reactions were initiated by the addition of 10 μL of ATP to a final ATP concentration of 10 μM and terminated after 60 min at room temperature by adding

20 μL of ADP reagent A and 40 μL of ADP reagent B. Compound 4 was used as a positive control. Compound dilutions were prepared from stock in DMSO and diluted with assay buffer for inhibition assay. The fluorescence signal detecting the amount of ADP produced as a result of enzyme activity was recorded on the Synergy 2 multimode microplate reader (BioTek) at an excitation wavelength of 530 nm and an emission wavelength of 590 nm at 30 min after the addition of the ADP reagent B. The inhibition rate (%) was calculated using the following equation:

$$\text{inhibition(\%)} = \left(1 - \frac{F_{590,\text{compd}}}{F_{590,\text{control}}}\right) \times 100 \quad (2)$$

IC₅₀ values were determined from the results of at least three independent tests and calculated from the inhibition curves. The accuracy of the in vitro screening assays was confirmed by the IC₅₀ value of control inhibitor 4 at 10 nM, which is in compliance with the reported value.²⁵

Kinase Profile. Tyrosine kinase profiling was performed using an ELISA based method as described previously.²⁶ Serine/threonine kinase profiling was performed at Shanghai ChemPartner Co., Ltd. according to the manufacturer's protocols. ATP concentrations in the kinase assay were at the K_m for each enzyme.

MTT Assays. Cell proliferation was measured by MTT assay as previously described.²⁷ Five thousand HCT116, MCF-7, and MDA-MB-231 cells in 100 μL of indicated medium were seeded in a 96-well plate in the presence of compounds at the indicated concentration. After incubation for 48 h, the cells were further incubated with 10 μL of 5 mg/mL MTT for 4 h at 37 °C in a humidified incubator with 5% CO₂. Then the formazan crystals were dissolved in 100 μL of DMSO, and the absorbance was measured at 570 nm by using a Synergy 2 multimode

Table 2. Selectivity Profile of Compounds 7 and 8 against a Panel of 21 Protein Kinases

tyrosine protein kinase	inhibition (%) for compd ^a		
	7	8	4
Flt-1	12.5	2.4	73.2
KDR	21.9	16.9	74.4
c-Kit	11.5	15.6	58.0
PDGFR- α	1.4	-6.9	32.6
PDGFR- β	55.2	32.4	62.8
RET	0.6	10.0	71.8
EGFR	44.9	32.4	36.6
c-Src	8.2	14.2	37.4
ABL	7.4	8.6	37.9
EPH-A2	24.0	38.2	70.7
FGFR1	15.5	31.3	61.2

serine/threonine protein kinase	inhibition (%) for compd ^b		
	7	8	4
AKT1	-2.5	8.6	NA
ERK1 (ERK2)	-4.4	2.8	NA (3)
GSK3 α (GSK3 β)	3.5	29.3	NA (95)
JNK2 (JNK1)	-1.4	11.0	NA (5)
MSK1	3.1	10.1	98
P38 α	2.7	13.0	16
p70S6K	6.2	6.9	94
PDK1	-16.8	-5.8	16
PIM1	86.8	0.7	NA
PKCa	-0.4	-22.0	97
RSK2	95.5	89.2	98

^aThe inhibitory percentage data of compounds 7, 8, and reference compound 4 against each tyrosine protein kinase at 10 μ M, which were determined by the mean value of at least two independent tests. ^bThe inhibitory percentage data of compounds 7 and 8 against the serine/threonine protein kinases excluding RSK2 at 10 μ M were determined through the kinase profiling service from Shanghai ChemPartner Co., Ltd. The data of control compound 4 against the serine/threonine protein kinases at 1 μ M are from ref 36.

microplate reader (BioTek). The inhibition rate (%) was calculated as follows:

$$\text{inhibition (\%)} = \left(1 - \frac{A_{570, \text{compd}}}{A_{570, \text{control}}} \right) \times 100 \quad (3)$$

IC₅₀ values were determined from the results of at least three independent tests and calculated from the inhibition curves.

In Vitro Pull-Down Assay with 7–Sephacryl 4B Beads. In vitro pull-down assay was done as previously described.²⁸ Compound 7 was coupled to a CNBr-activated Sepharose 4B beads according to the manufacturer's suggested protocol. The bacterial-expressed recombinant truncated and full-length RSK2 protein (aa44–367, aa1–740, 2 μ g) or endogenous HCT116 cell lysates (500 μ g) were incubated with 100 μ L of compound 7 coupled Sepharose 4B beads (50% slurry) in 400 μ L of reaction buffer (50 mM Tris, pH 7.5, 5 mM EDTA, 100 mM NaCl, 1 mM DTT, 0.01% NP40, 2 μ g/mL bovine serum albumin, 1 mM PMSF, 1% protease inhibitor mixture) overnight at 4 $^{\circ}$ C. The beads were washed five times with buffer (50 mM Tris, pH 7.5, 5 mM EDTA, 100 mM NaCl, 1 mM DTT, 0.01% NP40, 1 mM PMSF) and suspended

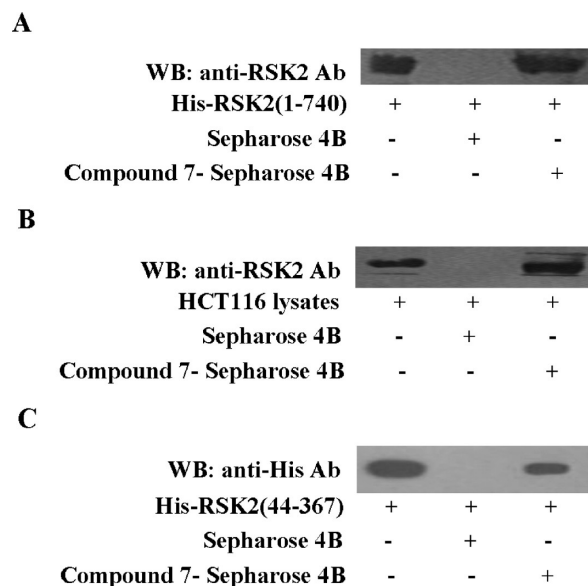


Figure 2. Immunoblotting analysis of pull-down assay indicates that compound 7 specifically binds with NTKD of RSK2: (A) bacterial-expressed full length RSK2 (aa1–740), (B) HCT116 lysates, and (C) bacterial-expressed NTKD of RSK2 (aa44–367).

in 40 μ L of 2 \times SDS loading buffer. Bind proteins were resolved by 10% SDS–PAGE and analyzed by Western blot using RSK2 antibody or His specific antibodies.

Western Blotting. For Western blotting assay, 2 \times 10⁵ cells were cultured in a six-well plate for 18 h and then starved in 0.1% FBS-DMEM for 18 h. The cells were then treated with compound 7 for 2 h and stimulated for 30 min with 10 ng/mL TPA. Cells were washed twice with ice-cold PBS and lysed in buffer containing 20 mM Tris (pH 7.5), 150 mM NaCl, 1% Triton X-100, 1 mM PMSF, supplemented with protease and phosphatase inhibitors (Sigma). The lysates were cleared by centrifugation at 10000g for 10 min at 4 $^{\circ}$ C, resolved by 10% SDS–PAGE, and then transferred to a PVDF membrane (Millipore). After transfer, the membrane was blocked in TBST buffer with 5% BSA at room temperature for 1 h. Blots were probed with the indicated primary antibody and horseradish-peroxidase-conjugated secondary antibody and were visualized and quantified using ECL Plus reagent (GE). The anti-RSK2 and anti-His antibodies were obtained from Santa Cruz. The anti-CREB, anti-p-CREB (Ser133), anti-GSK3 β , and anti-p-GSK3 β (Ser9) were purchased from Bioworld. Secondary antibodies were obtained from Jackson ImmunoResearch.

Wound Healing Assay. The migration of tumor cells was determined by scratch wound healing assay. MDA-MB-231 cells were seeded in a six-well plate and grown for 24 h to confluence. The monolayer cells were scratched with a 200 μ L yellow pipet tip to make a straight wound, and cells were washed with DMEM medium and then incubated with DMEM medium without serum. Then cells were treated with compound 7 in the indicated concentration for 48 h. Migrating cells were photographed under phase contrast microscopy (Olympus) at 0 and 48 h, respectively.

RESULTS AND DISCUSSION

Of the 156 candidates tested, 16 compounds were identified with IC₅₀ < 20 μ M (as shown in Table 1). SHAFTS algorithm captured the shapes and the chemotypes of the two templates as the essential features to build query models for scaffold hopping and to circumvent the intuitive similarities according to the atom environments and bond frameworks; the algorithm is superior to

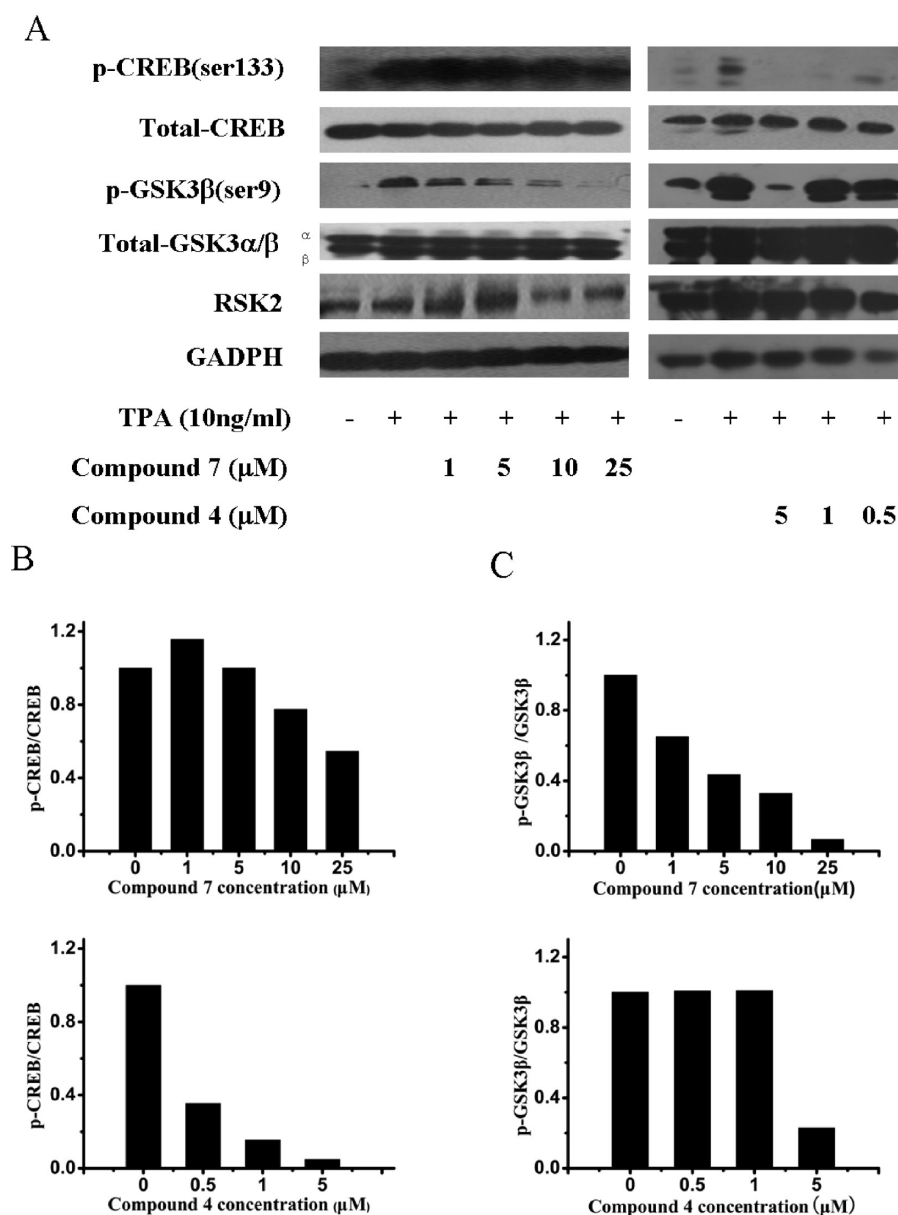


Figure 3. Compound 7 can block RSK2 mediated phosphorylation of the downstream substrate proteins. (A) Immunoblotting analysis of phosphorylation blocking effect of 7 for CREB and GSK3 β in the HCT116 cells lysates. Quantitative measurement of the levels of RSK2 mediated phosphorylation for (B) CREB and (C) GSK3 β along with compound 7 at various concentration gradients. Compound 4 was used as the reference RSK2 inhibitor.

the conventional 2D substructure/similarity searching. To make a direct comparison between the 2D similarity and the other shape-based 3D similarity methods and SHAFTS, we also calculate the 2D similarities of the hits to the corresponding queries with ECFP₄ fingerprint implemented in Pipeline Pilot (Accelrys Inc.), MACCS fingerprint implemented in OpenBabel (<http://openbabel.org/>), and ROCS “combo score” (OpenEye Inc.). As shown in Table 1, the highest similarity indexes of ECFP₄ and MACCS fingerprints for compound 12, for which the SHAFTS similarity value is 1.276, only have the values of 0.3 and 0.6, respectively (identical structures would have a value of 1.0), implying that the 2D similarities between the SHAFTS hits and the queries templates are relatively low. On the other hand, although the 16 active compounds had a 3D hybrid similarity in the range of 1.0–1.5 (identical structures would have a value

of 2.0 in SHAFTS), there were 759 candidates identified by SHAFTS in SPECS database in total (for two templates). However, as a point of reference, there are 1750 molecules in the same vendor catalogue with MACCS similarity values greater than the maximum value of 0.6 but less than five molecules with ECFP₄ index greater than 0.3 (data not shown). Moreover, most of the ROCS combo similarities are relatively lower than 1.0, indicating that it is unlikely to identify the same scaffolds in our study by ROCS if the similarity cutoff is also set to 1.0. As a result, the scaffolding hopping potential of SHAFTS can be highlighted when comparing with conventional 2D and 3D similarity methods.

Moreover, SHAFTS is more powerful than the conventional 2D methods as a ligand-based strategy for hit identification and subsequent hit-to-lead optimization because the overlays

Table 3. In Vitro Antiproliferation Activity of Selective RSK2 Inhibitors^a

compd	HCT116		MCF-7		MDA-MB-231	
	inhibition (%)	IC ₅₀ (μM)	inhibition (%)	IC ₅₀ (μM)	inhibition (%)	IC ₅₀ (μM)
7	89.64	30.2	98.29	25.5	89.24	16.12
8	91.64	56.23	97	17.98	98.83	14.88
9	13.16	ND	31.16	ND	6.89	ND
10	32.57	ND	21.32	ND	45.77	ND
11	44.24	>100	45.10	>100	54.67	>100
12	49.06	>100	85.79	15.56	97.93	9.69
13	6.50	ND	3.60	ND	0	ND
14	43.24	>100	32.67	ND	46.52	>100
15	28.40	ND	36.74	ND	22.17	ND
16	6.98	ND	32.9	ND	18.52	ND
17	4.80	ND	0	ND	12.05	ND
4 ^b	95.23	0.84	95.27	1.96	97.14	1.77

^a Relative inhibition rates of antiproliferative activity were determined by MTT assays. The final concentration of the compounds is 100 μM. IC₅₀ values were determined from the results of at least three independent tests of HCT116, MCF-7, and MDA-MB-231 cell lines in antiproliferative assays. Attempts to determine IC₅₀ values were made if the inhibition rate at 100 μM was larger than 40%. ND: not determined. ^b Relative inhibition rates of antiproliferative activities for the control compound 4 were determined at 10 μM.

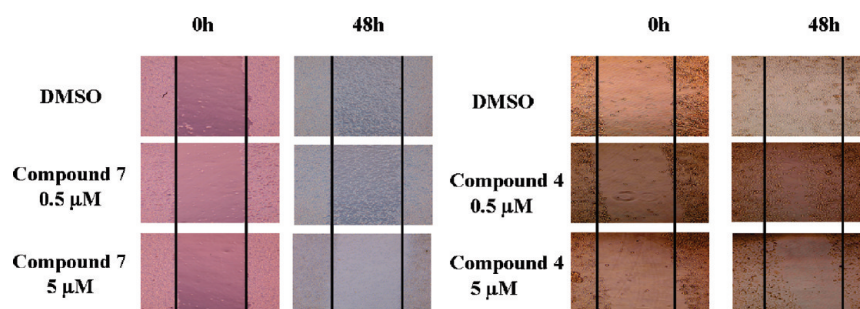


Figure 4. Compound 7 can suppress the migration of MDA-MB-231 cancer cell. Cells were scratched with a pipet tip and then treated with 0.5 and 5 μM 7 for 48 h. Migrating cells were photographed under phase contrast microscopy at 0 and 48 h. Compound 4 was used as the reference RSK2 inhibitor.

between the query and the hits can be explicitly visually analyzed, rendering it convenient for scaffold-hopping study. Figure 1 illustrates the superimposed poses of the three most active compounds 7–9 onto the corresponding templates based on the shape and chemical feature overlay. The hits have low molecular weights and rigid conformations. Although there is no experimental crystal structure for RSK2, which hinders in-depth exploration of the binding mode of the inhibitors, some putative pivotal interactions between the ligands and ATP-binding pocket in the homology model can be predicted (as shown in Figure 1). The binding modes of the template compounds 5 and 6 have been proposed with a homology model of RSK2 in an ATP-competitive way, in which the 7-hydroxyl group of 5 and 6 amino nitrogen and nitroso oxygen of 6 form the hydrogen bonds with Asp148 and Leu150 on the hinge region of the RSK2 NTKD.¹⁹ On the other hand, the amidine group of 5 and phenolic oxygen of 6 are hydrogen-bonded with Glu197. The proposed superimposed poses of these three hit compounds fitted pretty well on 5 or 6 in terms of both overall shape and pivotal chemical features observed in the cases of the templates: for example, one of the triazole nitrogens in 7 and lactam oxygen in 9 can form the hydrogen bonds with a hinge residue Leu150, while the amino group on the benzimidazole in 7 is hydrogen-bonded with another hinge residue Asp148. The other important

interaction mode predicted between the templates and Glu197 was also observed in the newly discovered inhibitors (as shown in Figure 1). Although some steric conflicts were also observed between the inhibitors and the ATP-binding pocket (like the case of compound 9), the overall accordance of the putative binding modes with the templates highlights the reliability and validity of SHATFS in this prospective virtual screening case study. The difference in inhibitory activities may be explained by the variance of the hydrogen bonds and shape complementary between the actives and RSK2.

To investigate the specificity and selectivity of these hits, we performed a selectivity profile against a panel of 21 protein kinases at 10 μM for the two most potent compounds 7 and 8. The kinase assay was done at the *K_m* of ATP for each kinase. As shown in Table 2, compounds 7 and 8 inhibit RSK2 at 10 μM but do not significantly inhibit other 21 tyrosine- and serine/threonine-kinases tested except Pim-1 kinase. These promising results from the kinase profile reveal that these two compounds may bear specific inhibitory activity for RSK2, although the Pim-1 kinase is inhibited by 7 to a similar extent as RSK2.

RSK2 consists of two nonidentical kinase domains, and inhibiting whichever of them suppresses the activation of RSK2 in vivo. Known RSK2 inhibitors like 1 and 2 especially inhibit RSK2 by competing for the ATP binding pocket at the

NTKD of RSK2, while **3** inactivates the CTKD of RSK2. The template compounds **5** and **6** used in this study were assumed to bind with the NTKD because they were discovered via virtual screening with a NTKD homology model. Hence, an effort was made to identify the specific binding domain of RSK2 for the hit compounds. To determine the molecular mechanism of compounds inhibition of RSK2, compound **7**, which was the most potent inhibitor in kinase assay, was selected for pull-down assay. We performed a pull-down assay with **7** conjugated to sepharose beads and bacterial-expressed full length RSK2 (aa1–740) and the endogenous RSK2 in HCT116 lysates. The results revealed that both recombinant full length RSK2 and endogenous RSK2 in HCT116 lysates are especially bound with **7** (Figure 2A and Figure 2B). Furthermore, bacterial-expressed NTKD of RSK2 (aa44–367) can also bind with **7** as shown in Figure 2C, indicating that the hit compound **7** can target the NTKD of RSK2 kinase in the intact cell.

To determine whether active compounds target the RSK2 *ex vivo*, compound **7** was selected for RSK2-mediated known downstream substrates phosphorylation assay. Two well-characterized downstream substrates of RSK2, CREB and GSK3 β , were immunoblotted with anti-phospho and anti-total protein antibody, respectively, with glyceraldehyde 3-phosphate dehydrogenase (GADPH) as the control for expression amounts. As shown in Figure 3, the result showed that compound **7** possesses strong inhibitory effect on the phosphorylation of GSK3 β in a dose-dependent manner. On the other hand, the inhibitory effect of compound **7** on the phosphorylation of CREB is not as strong as that of GSK3 β because CREB was reported as a dominant substrate for mitogen- and stress-activated protein kinase (MSK1) rather than RSK2.²⁹ Collectively, combined with the results from the kinase profile and pull down assay, the data demonstrate that compound **7** efficiently suppressed the phosphorylation of the downstream substrates like GSK3 β and CREB by directly inhibiting the RSK2 activation and subsequently alleviating the cellular signal transduction effects via RSK2.

RSK2 is a critical downstream effector in the RAS-ERK pathway and an effective regulator of cancer cell cycle^{30,31} and cell migration.^{9,10} The compounds that displayed inhibitory activities on RSK2 with an IC₅₀ less than 20 μ M were selected for the evaluation of antiproliferative potencies on three RSK2 overexpressed cancer cell lines (as shown in Table 3), and all of them demonstrated antiproliferation effects to some extent. The three most potent compounds **7–9** exhibited slight cytotoxicity toward the three cancer cell lines with IC₅₀ ranging from 14 to 88 μ M, which is similar to the antiproliferative activities of the known RSK2 inhibitors **1–3**.^{11,16,32} To elucidate the antimigration activities of RSK2 inhibitors, compound **7** was selected for a wound healing assay. Breast carcinoma MDA-MB-231 was scratched, and cells were treated with varied concentrations of compound **7** for 48 h. As illustrated in Figure 4, compound **7** suppressed the wound-healing migration of MDA-MB-231 cancer cells efficiently at 5 μ M, highlighting the role that RSK2 played in the migration of some human high metastasis tumors and the possibility of the hit compounds as the corresponding therapeutic agents. Since the antiproliferation or antimigration potency reflects both the binding affinity of the compound for the target protein and the ability to penetrate into the cells, the low antiproliferation activities of these hit compounds may be attributed to their poor penetration (as shown in Table S2). On the other hand, inhibiting RSK2 alone may not be necessarily sufficient to suppress the cellular proliferation and to drive the

cells into apoptosis because of the downstream effectors of RSK2 like NF- κ B, and CREB and GSK3 β have multiple key upstream regulators, including p38 MAPK,³³ MSK1,³⁴ and Akt kinases,³⁵ through which suppression of RSK2 mediated signal transduction may be offset or bypassed. As a remedy, combinatorial studies with other signaling inhibitors will be conducted in the future.

CONCLUSION

RSK2 plays a pivotal role in the regulation of diverse cellular processes, including cell proliferation, transformation, migration, and invasion. In this study, the hybrid 3D similarity calculation method SHAFTS was applied in the virtual screening study to identify novel potent RSK2 inhibitors. SHAFTS incorporates the shape overlay and pharmacophore feature matching the hybrid similarity and aligns the molecules in the multiconformers database onto the templates. Two weak RSK2 inhibitors were adopted as the query templates, and SHAFTS was used for rapid search of multiconformers databases to discover molecules with high SHAFTS similarities. By use of this procedure, 16 compounds with novel chemotypes (not similar to the queries in a 2D sense) were selected and described to bear RSK2 inhibitory activities. Further comparison study with ROCS and fingerprint-based 3D and 2D similarity methods highlighted the scaffold-hopping ability of SHAFTS. In fact, as a prospective study case, we intentionally selected RSK2 as the target because its crystal structure is not available currently, rendering it difficult to discover and optimize the novel inhibitor in a conventional structure-based way. In practice, we proved that taking both molecular shape and chemical features synergetically is a powerful and efficient method to perform scaffold-hopping without non-druglike and potential intellectual property issues as the query.

Moreover, the most potent hit compounds target RSK2 specifically with low micromolar inhibitory activities. In particular, compound **7** possesses strong *ex vivo* and *in vitro* RSK2 binding ability and also exhibits potent antimigration activity against the MDA-MB-231 tumor cell. We believe the hit compounds discovered in this work provide novel scaffolds for further hit-to-lead optimization and also lay the foundation for uncovering new RSK2 regulatory mechanisms.

ASSOCIATED CONTENT

S Supporting Information. Detailed description of SHAFTS algorithm; figure showing “quasi bioactive conformers” for the two template compounds **5** and **6**; table of HPLC analysis data of the 16 hits; rankings from the virtual screening results; and table listing *in silico* predicted druglike properties of the 16 compounds. This material is available free of charge via the Internet at <http://pubs.acs.org>.

AUTHOR INFORMATION

Corresponding Author

*For K.L.: phone, 86-371-67781959; fax, 86-371-67781959; e-mail, kdliu@zzu.edu.cn. For J.H.: phone, 86-21-64253681; fax, 86-21-64253681; e-mail, huangjin@ecust.edu.cn. For H.L.: phone, 86-21-64250213; fax, 86-21-64250213; e-mail, hlli@ecust.edu.cn.

Author Contributions

⁵These authors contributed equally to this work.

ACKNOWLEDGMENT

This work was supported by the Fundamental Research Funds for the Central Universities, the National Natural Science Foundation of China (Grants 20803022, 90813005, and 10979072), the Special Fund for Major State Basic Research Project (Grant 2009CB918501), the Shanghai Committee of Science and Technology (Grants 09dZ1975700 and 10431902600), the Innovation Program of Shanghai Municipal Education Commission (Grant 10ZZ41), the 863 Hi-Tech Program of China (Grant 2007AA02Z304), the 111 Project (Grant B07023), and the National S&T Major Project of China (Grants 2011ZX09307-002-03, 2009ZX09501-001, and 2009ZX09301-001). H.L. is sponsored by Shanghai Rising-Star Program (Grant 10QA1401800) and Program for New Century Excellent Talents in University. The authors appreciate Dr. Hua Xie and Linjiang Tong for the tyrosine protein kinase profile, and Zhongyu Xu for the compound purification analysis.

ABBREVIATIONS USED

RSK2, p90 ribosomal S6 protein kinase 2; MAPK, mitogen-activated protein kinase; ERK1/2, extracellular signal-regulated kinase-1 and -2; PDK-1, 3-phosphoinositide-dependent protein kinase-1; ER α , estrogen receptor- α ; NFAT3, nuclear factor of activated T-cells 3; ATF4, activating transcription factor 4; CLS, Coffin–Lowry syndrome; NTKD, N-terminal kinase domain; CTKD, C-terminal kinase domain; GSK3 β , glycogen synthase kinase-3 β ; CREB, cyclic AMP response element-binding protein; TPA, phorbol 12-myristate 13-acetate; GADPH, glyceraldehyde 3-phosphate dehydrogenase; MSK1, stress-activated protein kinase

REFERENCES

- (1) Carriere, A.; Ray, H.; Blenis, J.; Roux, P. P. The RSK factors of activating the Ras/MAPK signaling cascade. *Front. Biosci.* **2008**, *13*, 4258–4275.
- (2) Dalby, K. N.; Morrice, N.; Caudwell, F. B.; Avruch, J.; Cohen, P. Identification of regulatory phosphorylation sites in mitogen-activated protein kinase (MAPK)-activated protein kinase-1a/p90rsk that are inducible by MAPK. *J. Biol. Chem.* **1998**, *273*, 1496–1505.
- (3) Jones, S. W.; Erikson, E.; Blenis, J.; Maller, J. L.; Erikson, R. L. A *Xenopus* ribosomal S6 kinase has two apparent kinase domains that are each similar to distinct protein kinases. *Proc. Natl. Acad. Sci. U.S.A.* **1988**, *85*, 3377–3381.
- (4) Fisher, T. L.; Blenis, J. Evidence for two catalytically active kinase domains in pp90rsk. *Mol. Cell. Biol.* **1996**, *16*, 1212–1219.
- (5) Yang, X. G.; Matsuda, K.; Bialek, P.; Jacquot, S.; Masuoka, H. C.; Schinke, T.; Li, L. Z.; Brancorsini, S.; Sassone-Corsi, P.; Townes, T. M.; Hanauer, A.; Karsenty, G. ATF4 is a substrate of RSK2 and an essential regulator of osteoblast biology: implication for Coffin–Lowry syndrome. *Cell* **2004**, *117*, 387–398.
- (6) Xing, J.; Ginty, D. D.; Greenberg, M. E. Coupling of the RAS-MAPK pathway to gene activation by RSK2, a growth factor-regulated CREB kinase. *Science* **1996**, *273*, 959–963.
- (7) Joel, P. B.; Traish, A. M.; Lannigan, D. A. Estradiol-induced phosphorylation of serine 118 in the estrogen receptor is independent of p42/p44 mitogen-activated protein kinase. *J. Biol. Chem.* **1998**, *273*, 13317–13323.
- (8) Cho, Y. Y.; Yao, K.; Bode, A. M.; Bergen, H. R.; Madden, B. J.; Oh, S. M.; Ermakova, S.; Kang, B. S.; Choi, H. S.; Shim, J. H.; Dong, Z. G. RSK2 mediates muscle cell differentiation through regulation of NFAT3. *J. Biol. Chem.* **2007**, *282*, 8380–8392.
- (9) Doehn, U.; Hauge, C.; Frank, S. R.; Jensen, C. J.; Duda, K.; Nielsen, J. V.; Cohen, M. S.; Johansen, J. V.; Winther, B. R.; Lund, L. R.; Winther, O.; Taunton, J.; Hansen, S. H.; Frodin, M. RSK is a principal

effector of the RAS-ERK pathway for eliciting a coordinate promotile/invasive gene program and phenotype in epithelial cells. *Mol. Cell* **2009**, *35*, S11–S22.

- (10) Smolen, G. A.; Zhang, J.; Zubrowski, M. J.; Edelman, E. J.; Luo, B.; Yu, M.; Ng, L. W.; Scherber, C. M.; Schott, B. J.; Ramaswamy, S.; Irimia, D.; Root, D. E.; Haber, D. A. A genome-wide RNAi screen identifies multiple RSK-dependent regulators of cell migration. *Genes Dev.* **2010**, *24*, 2654–2665.

- (11) Kang, S.; Elf, S.; Lythgoe, K.; Hitosugi, T.; Taunton, J.; Zhou, W.; Xiong, L.; Wang, D.; Muller, S.; Fan, S.; Sun, S. Y.; Marcus, A. I.; Gu, T. L.; Polakiewicz, R. D.; Chen, Z. G.; Khuri, F. R.; Shin, D. M.; Chen, J. p90 ribosomal S6 kinase 2 promotes invasion and metastasis of human head and neck squamous cell carcinoma cells. *J. Clin. Invest.* **2010**, *120*, 1165–1177.

- (12) Kang, S.; Chen, J. Targeting RSK2 in human malignancies. *Expert Opin. Ther. Targets* **2011**, *15*, 11–20.

- (13) Nguyen, T. L. Targeting RSK: an overview of small molecule inhibitors. *Anti-Cancer Agents Med. Chem.* **2008**, *8*, 710–716.

- (14) Smith, J. A.; Maloney, D. J.; Clark, D. E.; Xu, Y. M.; Hecht, S. M.; Lannigan, D. A. Influence of rhamnose substituents on the potency of SL0101, an inhibitor of the Ser/Thr kinase, RSK. *Bioorg. Med. Chem.* **2006**, *14*, 6034–6042.

- (15) Smith, J. A.; Maloney, D. J.; Hecht, S. M.; Lannigan, D. A. Structural basis for the activity of the RSK-specific inhibitor, SL0101. *Bioorg. Med. Chem.* **2007**, *15*, 5018–5034.

- (16) Smith, J. A.; Poteet-Smith, C. E.; Xu, Y. M.; Errington, T. M.; Hecht, S. M.; Lannigan, D. A. Identification of the first specific inhibitor of p90 ribosomal S6 kinase (RSK) reveals an unexpected role for RSK in cancer cell proliferation. *Cancer Res.* **2005**, *65*, 1027–1034.

- (17) Sapkota, G. P.; Cummings, L.; Newell, F. S.; Armstrong, C.; Bain, J.; Frodin, M.; Grauert, M.; Hoffmann, M.; Schnapp, G.; Steegmaier, M.; Cohen, P.; Alessi, D. R. BI-D1870 is a specific inhibitor of the p90 RSK (ribosomal S6 kinase) isoforms in vitro and in vivo. *Biochem. J.* **2007**, *401*, 29–38.

- (18) Cohen, M. S.; Zhang, C.; Shokat, K. M.; Taunton, J. Structural bioinformatics-based design of selective, irreversible kinase inhibitors. *Science* **2005**, *308*, 1318–1321.

- (19) Nguyen, T. L.; Gussio, R.; Smith, J. A.; Lannigan, D. A.; Hecht, S. M.; Scudiero, D. A.; Shoemaker, R. H.; Zaharevitz, D. W. Homology model of RSK2 N-terminal kinase domain, structure-based identification of novel RSK2 inhibitors, and preliminary common pharmacophore. *Bioorg. Med. Chem.* **2006**, *14*, 6097–6105.

- (20) Liu, X. F.; Ouyang, S. S.; Yu, B. A.; Liu, Y. B.; Huang, K.; Gong, J. Y.; Zheng, S. Y.; Li, Z. H.; Li, H. L.; Jiang, H. L. PharmMapper server: a Web server for potential drug target identification using pharmacophore mapping approach. *Nucleic Acids Res.* **2010**, *38*, W609–W614.

- (21) Specs: Chemistry Solutions for Drug Discovery. <http://www.specs.net/> (accessed March 1, 2010).

- (22) MayBridge Screening Collection. <http://www.maybridge.com/> (accessed March 1, 2010).

- (23) *LigPrep*, version 2.0; Schrödinger, LLC: New York, NY, 2005.

- (24) Liu, X. F.; Bai, F.; Ouyang, S. S.; Wang, X. C.; Li, H. L.; Jiang, H. L. Cyndi: a multi-objective evolution algorithm based method for bioactive molecular conformational generation. *BMC Bioinf.* **2009**, *10*, 101.

- (25) Alessi, D. R. The protein kinase C inhibitors Ro31-8220 and GF109203X are equally potent inhibitors of MAPKAP kinase-1 β (Rsk-2) and p70 S6 kinase. *FEBS Lett.* **1997**, *402*, 121–123.

- (26) Liu, X. F.; Xie, H.; Luo, C.; Tong, L. J.; Wang, Y.; Peng, T.; Ding, J.; Jiang, H. L.; Li, H. L. Discovery and SAR of thiazolidine-2,4-dione analogues as insulin-like growth factor-1 receptor (IGF-1R) inhibitors via hierarchical virtual screening. *J. Med. Chem.* **2010**, *53*, 2661–2665.

- (27) Cho, Y. Y.; Yao, K.; Pugliese, A.; Malakhova, M. L.; Bode, A. M.; Dong, Z. G. A regulatory mechanism for RSK2 NH2-terminal kinase activity. *Cancer Res.* **2009**, *69*, 4398–4406.

- (28) Lee, K. M.; Lee, K. W.; Byun, S.; Jung, S. K.; Seo, S. K.; Heo, Y. S.; Bode, A. M.; Lee, H. J.; Dong, Z. 5-Deoxykaempferol plays a

potential therapeutic role by targeting multiple signaling pathways in skin cancer. *Cancer Prev. Res.* **2010**, *3*, 454–465.

(29) Deak, M.; Clifton, A. D.; Lucocq, L. M.; Alessi, D. R. Mitogen- and stress-activated protein kinase-1 (MSK1) is directly activated by MAPK and SAPK2/p38, and may mediate activation of CREB. *EMBO J.* **1998**, *17*, 4426–4441.

(30) Fujita, N.; Sato, S.; Tsuruo, T. Phosphorylation of p27(Kip1) at threonine 198 by p90 ribosomal protein S6 kinases promotes its binding to 14-3-3 and cytoplasmic localization. *J. Biol. Chem.* **2003**, *278*, 49254–49260.

(31) Palmer, A.; Gavin, A. C.; Nebreda, A. R. A link between MAP kinase and p34(cdc2)/cyclin B during oocyte maturation: p90(rsk) phosphorylates and inactivates the p34(cdc2) inhibitory kinase Myt1. *EMBO J.* **1998**, *17*, 5037–5047.

(32) Clark, D. E.; Errington, T. M.; Smith, J. A.; Frierson, H. F.; Weber, M. J.; Lannigan, D. A. The serine/threonine protein kinase, p90 ribosomal S6 kinase, is an important regulator of prostate cancer cell proliferation. *Cancer Res.* **2005**, *65*, 3108–3116.

(33) Xing, J.; Kornhauser, J. M.; Xia, Z.; Thiele, E. A.; Greenberg, M. E. Nerve growth factor activates extracellular signal-regulated kinase and p38 mitogen-activated protein kinase pathways to stimulate CREB serine 133 phosphorylation. *Mol. Cell. Biol.* **1998**, *18*, 1946–1955.

(34) Wiggin, G. R.; Soloaga, A.; Foster, J. M.; Murray-Tait, V.; Cohen, P.; Arthur, J. S. C. MSK1 and MSK2 are required for the mitogen- and stress-induced phosphorylation of CREB and ATF1 in fibroblasts. *Mol. Cell. Biol.* **2002**, *22*, 2871–2881.

(35) Shaw, M.; Cohen, P. Role of protein kinase B and the MAP kinase cascade in mediating the EGF-dependent inhibition of glycogen synthase kinase 3 in Swiss 3T3 cells. *FEBS Lett.* **1999**, *461*, 120–124.

(36) Davies, S. P.; Reddy, H.; Caivano, M.; Cohen, P. Specificity and mechanism of action of some commonly used protein kinase inhibitors. *Biochem. J.* **2000**, *351*, 95–105.